Dendrimer−Tetrachloroplatinate Precursor Interactions. 1. Hydration of Pt(II) Species and PAMAM Outer Pockets

Francisco Tarazona-Vasquez and Perla B. Balbuena*

Department of Chemical Engineering, Texas A&M University, College Station, Texas 77843

Received: August 3, 2006; In Final Form: November 8, 2006

Density functional theory is used to investigate the structure and energetics of the tetrachloroplatinate anion and its hydrolysis products at several degrees of hydration, as well as those of outer dendrimer pockets hosting such species. The number of water molecules able to saturate an unprotonated outer dendrimer pocket is found to be two, as inferred from calculated thermodynamic data. However, such a number could not be established for a protonated pocket where the dendrimer adopts a more open configuration. An analysis of possible pocket configurations is done on the basis of the orientations of the amide O atoms in the outer pockets. The effect of explicit water on the infrared spectra of the dendrimer pockets is reported and compared to experimental values.

1. Introduction

Nanotechnology has grown in importance because of its promising applications in many technological and scientific areas, especially in electronics[1] and catalysis.[2] Controlled design of nanoparticles is one of the vanguard areas of research in catalysis and involves an exhaustive analysis of materials and manufacturing processes. Because it is desirable that catalysts be highly active and efficient, a good catalytic design requires a thorough understanding of the processes involved in catalyst manufacturing, so that the design may be improved and controlled with more ease.

Metal nanoparticles used as nanocatalysts can be obtained through a number of techniques.[3,4] Templated synthesis with tetrachlorometallate alkaline salts as precursors in the liquid phase has been extensively used in the production of Pt, Pd, and bimetallic PtPd nanoparticles.[5−9] The study of small nanoclusters generated by these techniques has recently received attention.[10−12]

The small size of the nanocatalyst poses a challenge to its fabrication because sintering may take place during calcination treatment[13] or even at reaction conditions.[14] Therefore, a comprehensive study of the interactions between precursor molecules and the substrate—or template—where nanoparticles nucleate and grow may prove useful as those interactions are most likely to influence the processes involved in the evolution of the nanocatalyst structure and, consequently, of its physical and chemical properties. In templated synthesis of nanoparticles one such process is the complexation of the metal precursor with the host molecule, for example, a dendrimer. A dendrimer is a macromolecule composed of a core molecule, repetitive units (branches) stemming from a common point (branching point) in a dendrite-like manner, and terminated with surface groups such as $-NH_2$ and $-OH$. The following nomenclature is generally used to name a dendrimer: G*x*-S, where "G" stands for "generation" closely related to *x*, the number of "layers" of branches (minus one) grown from the core molecule, and "S" stands for the surface group. Thus, a G0-OH dendrimer is the simplest and smallest $-OH$ terminated dendrimer because it has a number of branches equal to the number of branching points (four as the core molecule is ethylenediamine (EDA)); G1-OH grows a "layer" of branches (eight branches) upon G0-OH; in G2-OH 16 more branches are added upon G1-OH, and so forth.

Little is known about how and to what extent complexation and related reactions are affected by environmental factors. However, the effect of the pH on the dendrimer structure has been determined:[15] this effect depends on the nature of the dendrimer terminal group. It is also known that, upon dissolution, the precursor salt K_2PtCl_4 hydrolyzes in aqueous solution as $PtCl_3(H_2O)^-$ and $PtCl_2(H_2O)_2$ depending on its initial concentration. Salt hydrolysis yields also ions such as K^+ and Cl^- that can affect the binding of metallic precursor species. Although Pt(II) and Pd(II) tetrachloroplatinate are extensively used as precursors,[5,16] in this work we focus our study only on Pt(II) precursors.

We perform quantum mechanical density functional theory (DFT) calculations on model systems. In order to gain insights about the effect of the pH and solvent on outer pockets, we model hydroxyl-terminated PAMAM poly(amidoamine) dendrimer environments. Regarding the effect of pH, our present molecular model of an outer pocket cannot describe the changes in the complete dendrimer configuration as a function of pH, as previously reported in experimental studies.[15] Nonetheless, any configurational change in the pockets should propagate to the global configuration of the dendrimer, even if the pockets are located in the dendrimer periphery. Experimentally, a progressive protonation of tertiary amine sites has been observed as the pH was decreased. However, at a given pH—around 3—protonation is total and a further decrease in pH does not seem to promote further protonation.[17] Therefore, it is clear that two scenarios can be targeted: the absence and presence of proton on tertiary amine sites. Some IR spectral features are reported and discussed in relation to previous work.[18] A high pH scenario cannot be considered here; the binding of hydroxyl ions to pockets is addressed elsewhere.[19] Also, because the dendrimer surrounding medium does not have a well-defined dielectric constant, a continuum model is not a convenient representation

* To whom correspondence should be addressed. E-mail: balbuena@tamu.edu.

10.1021/jp065014r CCC: $37.00 © 2007 American Chemical Society
Published on Web 01/18/2007

of such a medium. We have tried to circumvent this by adding explicit water molecules inside the pocket, thus accounting for local solvent effect. Finally, we report and analyze the relative stability and structures of tetrachloroplatinate species and their hydrates upon interaction with water. This is relevant for further work[19] where we study the binding of the counterions (K^+, Cl^-) and tetrachloroplatinate anion and its hydrates to the dendrimer sites.

One of our aims in learning more about the conformation of Pt(II) complexes has been to elucidate details of their binding to water, because the extent of such binding may have an indirect impact on the dynamics of the outer pocket−precursor interaction. Thus, for a solvated Pt(II) complex that approaches the dendrimer pocket, we are interested in determining if their hydration waters may migrate out of the Pt(II) complex first coordination shell as the complex becomes closer to the dendrimer pocket: pocket−metal precursor interactions will ease conditions for precursor encapsulation insofar as the Pt(II) complex orients its weakly bound waters toward the pocket as it moves toward it. We are also interested in determining the number of waters that saturate a dendrimer pocket with the goal of analyzing the details (to be reported elsewhere) of the exchange of water for Pt(II) complexes inside the pocket.

Once we have characterized the hydration of the complexes and their interactions with the pocket sites, we discuss a general scheme of the possible pocket configurations based on the relative positions of their amide oxygen atoms, and the effect that such configurations may have on the dendrimer conformation for unprotonated and tertiary amine protonated pockets.

CHART 1: Pictorial Representation of a G2 Dendrimer Illustrating the Difference between Outer Pocket and One-Layer-Inner Pocket[a]

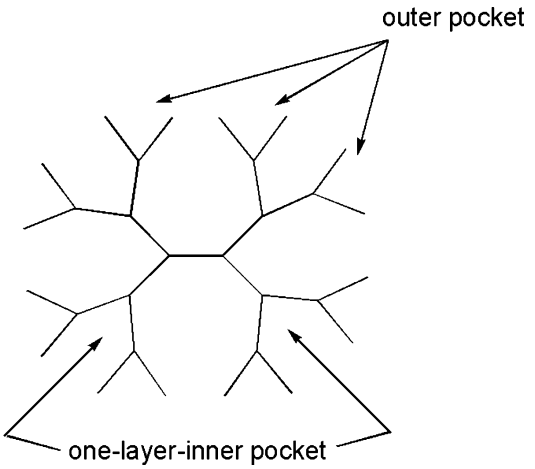

[a] Outer pockets are the outermost pockets delimited by two branches. One-layer-inner pockets are also delimited by two branches, but they are located closer to the core: the center of the dendrimer.

2. Models and Computational Procedures

We use the B3LYP hybrid flavor of DFT along with Hay and Wadt pseudopotentials[20] for Pt and 6-31+g(d) basis set for all other atoms. None of the calculated structures for $PtCl_4^{2-}$ and $PtCl_4^{2-}$−H_2O have stable states with spin multiplicities higher than 1. Although not all our modeled species are anions, for the sake of consistency we have used the same method and basis sets when calculating cations and neutral species. Two tests were done to validate the combination DFT functional/basis set. First, we tested the suitability of this combination to reproduce the proton affinity (PA) of $N(CH_3)_3$, trimethylamine. We obtained values of 222.8 kcal/mol for the proton affinity ($PA = -\Delta H_{rxn}$), whereas the available experimental value is 226.7 kcal/mol.[21]

Second, the suitability of combining B3LYP/6-31+g(d) for light atoms and Hay and Wadt relativistic pseudopotentials (LANL2DZ) for transition metal atoms was tested. Calculations for Ni hydrates were made with two basis sets: 6-31g(d) and 6-31+g(d). The gas-phase binding energy value calculated as $\Delta E_{9,10} = E([Ni(H_2O)_{10}]^{2+}) - E([Ni(H_2O)_9]^{2+}) - E(H_2O)$ was −11.10 kcal/mol for B3LYP/6-31g(d)/LANL2DZ. However, the value was −7.8 kcal/mol for B3LYP/6-31+g(d)/LANL2DZ, in excellent agreement with the reported experimental value[22] of −7.9 kcal/mol. Consequently, the adequacy of such a combination is suggested in this work, particularly for cationic species. A similar combination has been previously reported.[23] Nonetheless, we do not claim finding the absolute thermodynamic quantities for a given reaction. Rather, we evaluate relative energies and consider that they provide accurate insights into the feasibility of the reactions that take place upon interaction of the species with water molecules.

Although our study is not done in the condensed phase, we consider it an approximation in such a direction. The most obvious impact of the condensed phase on the dendrimer properties is that of the solvent. For instance, its polarity is expected to affect the conformation of a dendrimer in solution.[24] We chose water as a solvent because aqueous solutions of dendrimers are ubiquitous in templated nanoparticle synthesis where dendrimers are the host molecules. An important question relates to the distribution of water molecules once they enter the dendrimer. To answer this question, we first realize that a complete dendrimer, especially one of generation larger than G0, is intractable by current quantum mechanical (QM) methods. Fortunately, the interactions between any species and the dendrimer are more likely to be local because such species would have to overcome interactions with the dendrimer outer pockets before being able to reach the inner voids. This should be especially true in the early stages of their interactions (Chart 1). The effect of binding of water in a tertiary amine protonated pocket is also studied. We consider a pocket made out of two—rather than more than two—branches because computational demand scales with system size. Our outer pocket model is a good starting point toward understanding how strong the binding inside the pockets is and which dendrimer atoms participate in such binding.

Thermodynamic quantities (binding energy, enthalpy, and free energy) of the complexation process and the associated geometric properties (bond length, bond angles) of involved species were calculated by representing the outer pockets with suitable fragments. The DF nomenclature stands for "dendrimer fragment", and it is followed by the number of atoms that compose the fragment. Structurally, DF41 is similar to a fragment we used in previous work[25] consisting of two branches stemming from a tertiary amine nitrogen but completing the triple coordination with a methyl group rather than with a H atom. In addition, here we use DF41−H that has a proton on top of its tertiary amine.

The Gaussian03 suite of programs[26] was used to obtain optimized geometries corresponding to minimum energy configurations; the nature of the stationary points was tested with frequency calculations that also provide the zero point energy and the thermal and free energy corrections to the electronic energy within the harmonic approximation.

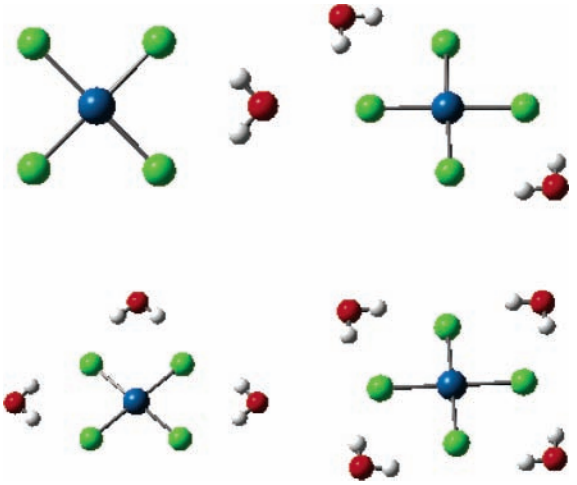

Figure 1. $PtCl_4^{2-}$ lowest energy configurations (nomenclature as in Table 1) at a given degree of hydration. Upper left: configuration 1A, $PtCl_4^{2-}-(H_2O)$. Upper right: configuration 2A, $PtCl_4^{2-}-(H_2O)_2$. Lower left: configuration 3A, $PtCl_4^{2-}-(H_2O)_3$. Lower right: configuration 4A, $PtCl_4^{2-}-(H_2O)_4$.

TABLE 1: Hydration of $PtCl_4^{2-}$ According to the Reaction $(PtCl_4^{2-})(H_2O)_n + (H_2O)_2 \rightarrow (PtCl_4^{2-})(H_2O)_{n+1} + H_2O$[a]

n	product config	ΔE_0	ΔH	ΔG
0	1A	−12.2	−12.0	−10.0
1	2A	−11.1	−10.9	−8.8
1	2B	−8.4	−8.4	−6.0
2	3A	−9.7	−9.8	−6.4
2	3B	−6.2	−6.9	−2.1
3	4A	−8.6	−7.6	−9.0
3	4B	−7.5	−7.3	−6.8
3	4D	−8.0	−8.3	−4.3
3	4F	−5.2	−5.4	−2.0
3	4I	−10.4	−11.6	−4.7

[a] Energies are given in kcal/mol.

3. Results

3.1. Tetrachloroplatinate Ion and Its Hydrates: Structure and Energies. Geometries and energetics for $PtCl_4^{2-}$ and its mono- and dihydrated byproducts are reported in this section. No symmetry constraints were imposed in the calculations.

3.1.1. $PtCl_4^{2-}$. Our thermodynamic calculations on the successive hydration of this molecule indicate that hydration is a favorable process, although the extent at which the solvent saturates the ion first shell cannot be precisely determined. At a given degree of hydration, several configurations were found (see Supporting Information), but only the lowest energy configurations (LECs) are shown in Figure 1. The optimized geometry of gas-phase $PtCl_4^{2-}$ is square planar as expected, with a Pt−Cl distance of 2.42 Å. These values are larger than the experimental bond distances in K_2PtCl_4 crystals reported to be 2.31 Å.[27] To aid in the description of the configurations shown in Figure 1, let us assume that there are six binding sites for the hydration of the square planar anion $PtCl_4^{2-}$. Four sites are in the plane of the molecule and we further refer to them as *equatorial*, while two more are above and below the central atom and we refer to them as *axial*. For $PtCl_4^{2-}-H_2O$, no water molecules are found in axial sites for the LEC; thus the water molecule occupies an equatorial site. For $PtCl_4^{2-}-(H_2O)_2$, two water molecules occupy diametrically opposed equatorial sites. This configuration, 2A (Table 1 and Figure 1), is more stable than 2B, where a water dimer is found above the plane with one water binding two adjacent Cl ligands while the other water molecule shifts slightly from an axial position (Pt−O(water) distance 4.08 Å). The O−H bond length is 0.98 Å and the angle H−O−H ranges from 98.9° to 99.8°, with smaller angles corresponding to lower degrees of hydration. For $PtCl_4^{2-}-(H_2O)_3$ the most stable configuration is that where water molecules occupy three equatorial sites (configuration 3A in Table 1 and Figure 1). A less stable configuration (3B) was found with a water trimer above the equatorial plane. Finally, for $PtCl_4^{2-}-(H_2O)_4$ four water molecules saturate the equatorial sites (configuration 4A in Table 1 and Figure 1). This configuration is more stable than 4B (Table 1), where two dimers occupy diametrically opposed equatorial sites. The next stable (4I) has a water tetramer on top of the molecule, but in none of these cases are isolated individual waters found in axial positions, in agreement with Ayala et al.,[28] who on the basis of the similarity between the XANES spectra of solid state and aqueous solutions of $PtCl_4^{2-}$ concluded that no water molecules can bind stably in the axial region. In any case, no oxygen was found directly coordinated with the Pt atom, although Table 1 shows that the difference in ΔG between the LEC and the next most stable configuration at each level of hydration is not large (2.8 kcal/mol between 2A and 2B, 4.3 kcal/mol between 3A and 3B, and 2.2 kcal/mol between 4A and 4B).

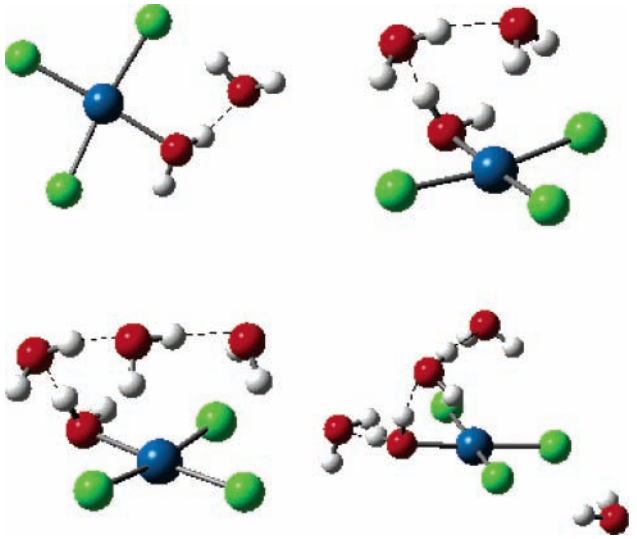

Figure 2. $PtCl_3(H_2O)^-$ lowest energy configurations at various degrees of hydration. Upper left: $PtCl_3(H_2O)^--(H_2O)$ with H-bond Pt−HOH···OH_2 at 1.76 Å. Upper right: $PtCl_3(H_2O)^--(H_2O)_2$ with H-bonds Pt−HOH···OH_2 at 1.72 Å and H_2O···OH_2 at 1.90 Å. Lower left: $PtCl_3(H_2O)^--(H_2O)_3$ with H-bond Pt−HOH···OH_2 at 1.66 Å and two H-bonds H_2O···OH_2 at 1.77 and 1.86 Å, respectively, over the molecular square plane. Lower right: $PtCl_3(H_2O)^--(H_2O)_4$ with H-bond Pt−HOH···OH_2 at 1.78 Å and two H-bonds H_2O···OH_2 at 1.74 and 1.89 Å, respectively, over the molecular square plane.

3.1.2. $PtCl_3(H_2O)^-$. The geometry of the complex deviates slightly from a square planar configuration. The average angle Cl−Pt−Cl, where the Cl^- ligands are located in the cis position with respect to each other, is 95°, whereas the average angle Cl−Pt−O, where the Cl^- and water ligand O are located in *cis* position with respect to each other, is 85°. The hydrogen atoms of water lay outside of the plane containing Pt, Cl, and water ligand O atoms.

The LECs upon hydration are shown in Figure 2 (all configurations are provided as Supporting Information). The Pt−Cl distance for the Cl^- ligand trans to the H_2O ligand ranges from 2.33 to 2.35 Å, whereas that for the Cl^- ligands cis to H_2O averages 2.40 Å. The Pt−O distance ranges from 2.13 to 2.18 Å, with the shortest value observed at a higher degree of

TABLE 2: Hydration of $PtCl_3(H_2O)^-$ According to the Reaction $(PtCl_3(H_2O)^-)(H_2O)_n + (H_2O)_2 \rightarrow (PtCl_3(H_2O)^-)(H_2O)_{n+1} + H_2O$[a]

n	config	ΔE_0	ΔH	ΔG
0	1A	−5.1	−4.7	−3.3
0	1B	−7.9	−8.3	−4.2
1	2A	−4.0	−3.5	−2.7
1	2B	−5.7	−5.8	−2.9
1	2C	−8.0	−8.1	−4.9
2	3A	−7.8	−8.1	−4.4
3	4A	2.1	3.4	1.3
3	4B	1.0	1.0	3.8
3	4C	−0.6	0.2	0.2

[a] Energies are given in kcal/mol.

hydration. The assumption of six binding sites still holds, although with different environments for each site, i.e., four equatorial sites but only two distinct ones: a site Cl−Cl located between two Cl^- ligands, as the four equatorial sites observed for $PtCl_4^{2-}$, and a site Cl−O located between a Cl^- and a water oxygen (Figure 2). We still consider axial sites those above and below the Pt atom.

For $PtCl_3H_2O^-$−H_2O, two different configurations for a water molecule occupying each distinct equatorial site are found; however, the LEC is that where water occupies the Cl−O site (Figure 2). This result hints that it could be easier to release water from a Cl−Cl site than from a Cl−O site. For $PtCl_3H_2O^-$−$(H_2O)_2$, three different stable configurations are found. In one of them, water molecules occupy both Cl−Cl sites; in another one, water occupies both Cl−O sites. However, the LEC is that where a water dimer is oriented across the molecular plane from a Cl−O site toward the diametrically opposed Cl−Cl site. For $PtCl_3H_2O^-$−$(H_2O)_3$, the LEC is a trimer on top of the molecular plane center, as was found in the case of the dimer (Figure 2). It resembles the LEC for $PtCl_3H_2O^-$−$(H_2O)_2$, but with one additional water inserted in the middle of the dimer.

For $PtCl_3H_2O^-$−$(H_2O)_4$, none of these structures has a negative ΔG of reaction (Table 2). However, the lowest positive ΔG is 0.2 kcal/mol (structure shown in Figure 2), which, considering the margin of error involved in DFT calculations, it could be thermodynamically feasible ($\Delta E_0 = -0.6$ kcal/mol), although this seems not as clear as in the case of $PtCl_4^{2-}$ discussed above.

Several water molecules, two or more, forming an H-bond network above the molecular plane have been found (as in the case of $PtCl_4^{2-}$), but none of the water molecules stays over the axial sites. In the configurations having dimers and trimers, the closest Pt−O distances are 3.31 and 3.56 Å, respectively, and 3.34 Å for the tetramer—comparable to 3.3 Å calculated previously.[28] In hydration water molecules the O−H bond length is 0.97−0.99 Å and the H−O−H angle ranges from 101.2° to 104.9°.

Although water in axial sites has been suggested for $Pt(H_2O)_4^{2+}$ [29] and its square planar analogue $Pd(H_2O)_4^{2+}$ [30] as well as for $PtCl_4^{2-}$,[31] even if such sites were binding sites, water molecules would not remain stable there.[28] Nonetheless, a clear line cannot be drawn: even in our calculations we found several water molecules—two or more—linked in a H-bond network above the molecular plane.

3.1.3. cis-$PtCl_2(H_2O)_2$. The geometry of this complex deviates from square planar, and it is at least of C_2 symmetry (Figure 3). The Cl−Pt−Cl angle is 98° and the O−Pt−O angle 95°. Each of the water ligands has a hydrogen atom in the molecular plane and one out of it. The out-of-plane hydrogen atoms are on opposite sides of the plane (above and below).

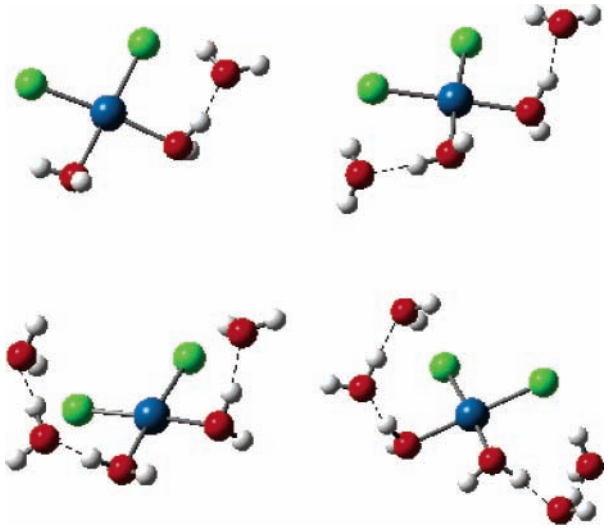

Figure 3. *cis*-$PtCl_2(H_2O)_2$ lowest energy configurations at a given degree of hydration. Upper left: *cis*-$PtCl_2(H_2O)_2$−(H_2O). There is an H-bond Pt−OH_2···OH_2 with length 1.67 Å. Upper right: *trans*-$PtCl_2$-$(H_2O)_2$−$(H_2O)_2$. Two H-bonds Pt−OH_2···OH_2 at 1.66 and 1.64 Å. Lower left: *trans*-$PtCl_2(H_2O)_2$−$(H_2O)_3$. Two H-bonds Pt−OH_2···OH_2 stemming from adjacent water ligands at 1.61 and 1.66 Å and one intersolvent H-bond HOH···O at 1.72 Å. Lower right: *trans*-$PtCl_2$-$(H_2O)_2$−$(H_2O)_4$. Two H-bonds Pt−OH_2···OH_2 stemming from adjacent water ligands at 1.60 and 1.61 Å and two H-bond networks above and below the complex (HOH···O) at 1.71 and 1.72 Å.

TABLE 3: Hydration of *cis*-$PtCl_2(H_2O)_2$ According to the Reaction $(cis\text{-}PtCl_2(H_2O)_2)(H_2O)_n + (H_2O)_2 \rightarrow (cis\text{-}PtCl_2(H_2O)_2)(H_2O)_{n+1} + H_2O$[a]

n	config	ΔE_0	ΔH	ΔG
0	1A	1.5	2.3	2.0
0	1B	−6.8	−7.1	−4.3
0	1C	−4.0	−3.9	−1.9
1	2A	0.9	1.9	2.0
1	2B	−7.3	−7.3	−4.9
1	2C	−5.4	−5.6	−2.4
2	3A	−4.4	−4.6	−0.9
2	3C	−3.8	−4.0	−0.2
3	4A	−7.6	−8.0	−3.2
3	4C	1.5	2.2	1.7
3	4E	−6.9	−6.9	−4.3

[a] Energies are given in kcal/mol.

Results (Table 3) on the successive hydration show that hydration is favored, although an upper limit could not be determined as the free energies obtained at the highest degree of hydration tested are still negative. The LECs upon hydration are shown in Figure 3 (all configurations are provided as Supporting Information).

The Pt−Cl bond distance ranges between 2.32 and 2.34 Å and that of Pt−O ranges between 2.13 and 2.16 Å. The assumption of six binding sites can be maintained, observing that there are three distinct sites in equatorial position: one Cl−Cl site and two Cl−O sites as described above, and an additional O−O located between the two water oxygen atoms belonging to water molecules located in cis positions to each other. Sites above and below the Pt atom continue to be referred to as *axial*. The LEC of *cis*-$PtCl_2(H_2O)_2$−H_2O is that where water occupies the Cl−O site, in the next stable configuration (higher in energy) water occupies the O−O site, and in the least stable water occupies the Cl−Cl site. This trend is similar to that observed for $PtCl_3(H_2O)^-$−H_2O. For the LEC of *cis*-$PtCl_2(H_2O)_2$−$(H_2O)_2$ each water occupies a Cl−O site; in the next stable configuration water molecules locate one in Cl−O and another in O−O sites,

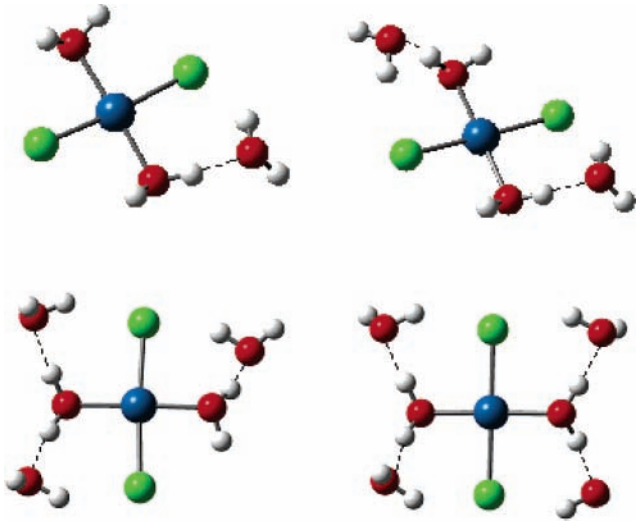

Figure 4. *trans*-$PtCl_2(H_2O)_2$ lowest energy configurations at a given degree of hydration. Upper left: *trans*-$PtCl_2(H_2O)_2-(H_2O)$. There is a hydrogen bond $Pt-OH_2\cdots OH_2$ at 1.63 Å. Upper right: *trans*-$PtCl_2(H_2O)_2-(H_2O)_2$. Two hydrogen bonds $Pt-OH_2\cdots OH_2$, both at 1.64 Å. Lower left: *trans*-$PtCl_2(H_2O)_2-(H_2O)_3$. Three H-bonds $Pt-OH_2\cdots OH_2$ with lengths 1.65, 1.70, and 1.71 Å. Lower right: *trans*-$PtCl_2(H_2O)_2-(H_2O)_4$. Four H-bonds $Pt-OH_2\cdots OH_2$ with lengths 1.70−1.72 Å.

whereas in the least stable configuration, they appear in Cl−Cl and Cl−O sites. For the LEC of *cis*-$PtCl_2(H_2O)_2-(H_2O)_3$ a water molecule occupies a Cl−O site and a water dimer occupies the other Cl−O site, and for *cis*-$PtCl_2(H_2O)_2-(H_2O)_4$, the LEC is that where each water dimer occupies a Cl−O site and the centers of mass of the dimers locate above and below the molecular plane. We did not observe configurations where water binds to axial positions. Perhaps they will become more evident as more water is added, but also the complexity of the local minima search increases. For water molecules the O−H bond length ranges from 0.97 to 1.00 Å and the HOH angle ranges from 105° to 107°.

3.1.4. trans-$PtCl_2(H_2O)_2$. Although the magnitude of the angles Cl−Pt−Cl and O−Pt−O (180°) guarantees that atoms other than hydrogen are in the same plane, the structure deviates slightly from square planar: the magnitudes of any pair of adjacent angles Cl−Pt−O are 95° and 85°. By taking one water ligand as reference, we observe that one of their hydrogen atoms is slightly off the plane pointing in a direction parallel to the closest Pt−Cl bond and forming an angle of 108° with the water oxygen and the other hydrogen atom so that this atom is outside the plane. The water molecules are trans to each other, having their slightly-off hydrogen atoms pointing in opposite directions and their out-of-plane hydrogen atoms above and below the molecular plane.

Deeth and Elding[32] calculated LDA geometries of several complexes—among them *trans*-$[PtCl_2(H_2O)_2]$—yielding bond lengths closer to available structural data (2.31 Å for the Pt−Cl distance in the $(NH_4)_2PtCl_4$ compound).[33] Our calculated *trans*-$PtCl_2(H_2O)_2$ geometry is similar to that reported by sketch 17, Figure 1 in ref 32, except that their reported Pt−O and Pt−Cl bond distances are 2.03 and 2.32 Å, respectively, whereas ours are 2.07 and 2.38 Å as an average for all structures regardless of the degree of hydration.

ΔG of hydration for the successive hydration reactions shows that hydration is favored. The LEC structures upon hydration are shown in Figure 4 (all configurations are provided as Supporting Information).

TABLE 4: Hydration of *trans*-$PtCl_2(H_2O)_2$ According to the Reaction (*trans*-$PtCl_2(H_2O)_2)(H_2O)_n + (H_2O)_2 \rightarrow$ (*trans*-$PtCl_2(H_2O)_2)(H_2O)_{n+1} + H_2O$[a]

n	config	ΔE_0	ΔH	ΔG
0	1A	−9.7	−9.9	−6.6
1	2A	−6.3	−6.2	−3.7
1	2B	−8.9	−9.1	−5.6
2	3Z	−4.7	−4.5	−2.8
2	3A	1.6	1.7	3.8
2	3B	−0.2	0.3	0.8
2	3C	−3.3	−3.7	0.5
2	3D	3.1	3.8	4.4
3	4A	−4.3	−4.9	0.2
3	4Z	−4.9	−4.7	−2.5

[a] Energies are given in kcal/mol.

TABLE 5: Differences in ΔE_0, ΔH, and ΔG between the Lowest Energy Configurations of *cis*- and *trans*-$PtCl_2(H_2O)_2\cdots(H_2O)_n$ with n_{hyd} the Number of Waters of Hydration[a]

n_{hyd}	$\Delta\Delta E_0$	$\Delta\Delta H$	$\Delta\Delta G$
0	0.25	0.29	0.80
1	3.1	3.0	3.0
2	4.6	4.9	3.7
3	4.9	4.8	5.6
4	1.7	1.6	2.2

[a] Energies (in kcal/mol) are given as $E_{cis} - E_{trans}$.

For this molecule, all four equatorial sites are Cl−O; sites above and below the center of the molecular plane continue to be referred to as *axial*. In *trans*-$PtCl_2(H_2O)_2-H_2O$, all four equatorial sites are equivalent, so only one conformer is found, whereas for *trans*-$PtCl_2(H_2O)_2-(H_2O)_2$, the LEC is the one where two waters occupy two diametrically opposed equatorial sites. For *trans*-$PtCl_2(H_2O)_2-(H_2O)_3$ the LEC is the one where three water molecules occupy three equatorial sites as seen in Figure 4; the next local minimum (3C) is the one where a water trimer is found above the molecular plane, bound via its peripheral water molecules to both water ligands, whereas the central water in the water trimer is also bound to one Cl^- ligand and its O atom is 3.60 Å from the Pt atom.

For *trans*-$PtCl_2(H_2O)_2-(H_2O)_4$, the LEC has all the equatorial sites occupied by water molecules. The next local minimum resembles closely the geometry of the three-water second lowest minimum described above, but with the addition of one water molecule to one of the ends of the water trimer. This added water molecule binds also to a Cl^- ligand. We do not observe O atoms in axial positions or O atoms coordinating directly to Pt. For the lower energy configurations the water of hydration parameters are O−H bond lengths of 0.97−0.98 Å and H−O−H angles ranging from 105.7° to 106.9°.

Comparison between structures of *cis*- and *trans*-$PtCl_2(H_2O)_2$ with similar degrees of hydration might provide insights into the predominant species in aqueous solution. From Table 5 it is observed that the trans isomer is more stable than the cis configuration. When there are no hydration waters this difference is minimal; it becomes a maximum at $n_{hyd} = 3$ and then decreases until the highest degree of hydration calculated by us ($n_{hyd} = 4$).

The experimental value for the equilibrium constant [cis]/[trans] is 1.2.[34] From the relationship between thermodynamics and the equilibrium constant is deduced that ΔG for the isomerization trans → cis is −0.1 kcal/mol. Therefore, a slight predominance of the cis isomer over trans in aqueous solutions is expected. However, it has also been stated[35] that in the gas phase the trans isomer is marginally more stable than the cis

isomer. This is in agreement with the trend observed in our calculations. Nonetheless, we are still unable to match the experimental result in aqueous solution. One reason might be that the maximum amount of explicit water used ($n_{hyd} = 4$) is still insufficient to describe a full-solvent effect. Despite the availability of a number of sampling techniques for free energy calculations—among which multicanonical and umbrella sampling are representative[36]—such a cis−trans energy difference would be extremely difficult to prove by any of the current implementations of molecular dynamics simulations due to the inherent limited time scale,[37] slow convergence,[36] and large number of simulations required,[38] and because the reproducibility error,[39] sampling accuracy,[40] and statistical uncertainty[38] are larger than the energy difference that has been reported experimentally.[34] Therefore, we leave the question open from the theoretical point of view.

Finally, as experimental and computational data seem to indicate that the cis−trans energy difference in bulk solvent is not significant, we include both *cis*- and *trans*-$PtCl_2(H_2O)_2$ species[19] in our study of dendrimer−metal precursor interactions to be reported elsewhere.

3.2. Pocket Orientation and the Configurational Issue. In this section we provide qualitative insights on the configuration of outer pockets even though there are no experimental data to compare our results. As stated in the Introduction, we argue that a continuum model is not a realistic approach to account for the solvent effect, because in a large dendrimer an outer pocket interacts with the bulk solution through its "mouth" (i.e., the space between the terminal groups of the branches) and therefore is not surrounded by an environment of uniform dielectric constant.

As the configuration of a dendrimer is altered by the presence of the solvent and pH among other factors, it is expected that cations/anions may also modify this configuration. ESI-MS experiments performed with small dendrimers have confirmed that counterions such as Na^+ can be found trapped inside the dendrimer.[10] However, such experiments could not provide a *detailed* description of the binding between cations/anions/water molecules and dendrimer atomic sites, nor did they offer insights about the nature of those sites. The use of molecular models and its resolution by QM methods can yield complementary information related to the identity of such sites and to their relative binding strengths. In this section we focus on understanding how the different species—particularly water and proton—present inside a dendrimer pocket influence its configuration, and consequently that of the dendrimer as stated in the Introduction.

3.2.1. Pocket Orientation and the Role of Amide-O Orientation on PAMAM Conformation. There are a number of configurations that a dendrimer might adopt as a function of generation. We illustrate this with a simple calculation while we discuss some substructures that could be formed as a consequence of the presence of cations/anions. The following assumptions are made: first, the configuration of all amide groups will remain trans;[18] second, there is no backfolding of branches, so the dendrimer extends ideally forming outer pockets limited by two branches and is reasonably planar (so this approach could not be extended to large generation dendrimers, especially to those spherical in shape). We postulate that configurations are to be determined on the basis of the orientation of the amide O atom.

In Chart 2, the horizontal central line represents the core of the dendrimer with the tertiary amine atoms located at the end of the line. We assumed the magnitude of the dihedral formed by the tertiary amines N3 and both methylene carbon atoms CN3 in the EDA core (core dihedral N3−CN3−CN3−N3) to be 180°. If a line (representing the innermost half of a branch) stemming from either extreme of that line is drawn, then the amide O atom can be found either to its right (1) or to its left (2). With four branches, the possible number of combinations is $2^4 = 16$, but if the molecule is considered to have a symmetry plane that coincides with the plane of the figure, then a configuration 1111 seen from above is identical to a 2222 seen from below such a plane. Therefore, only eight different configurations can be found for the core (Chart 2).

CHART 2: Orientation of Amide O Atoms in the Dendrimer Core[a]

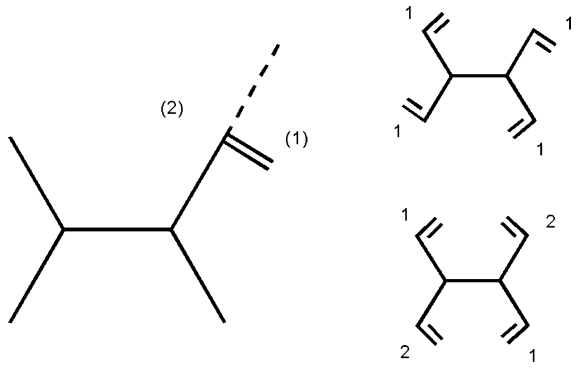

[a] Left side: amide O can be found in either of two positions with respect to its containing branch: "right" (1) when it lies at the right side of the dashed line (projected from the carbonyl C) and "left" (2) when the amide O lies at the left side of the same line. Right side: two (out of eight) examples of core configuration.

CHART 3: Orientation of Amide O in Outer Pockets[a]

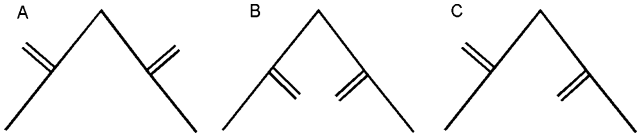

[a] (A) In both branches amide O atoms orient outwardly (outward−outward). (B) In both branches amide O atoms orient inwardly (inward−inward). (C) One amide O orients outwardly, while the other orients inwardly (outward−inward).

Next, we consider the orientation of the amide O in the outer pockets. There are at least three distinct ideal cases: when both amide O atoms orient outward from the pocket (Chart 3A, outward−outward), when both amide O atoms orient inward toward the pocket (Chart 3B, inward−inward), and when one amide O orients outward and the other inward (Chart 3C, outward−inward). In Chart 3, the lines represent the branch extending from the branching point toward the surface terminal group.

As G1-OH can be built from G0-OH plus four outer pockets, how many different configurations are then possible? We assume that each pocket can adopt any of the configurations (A, B, or C in Chart 3) independently of the configurations of the other pockets, so that, for instance, the configuration AAAB is different from AABA. Consequently, there are 3^4 possible configurations for the arrangement of four pockets having a fixed configuration for the dendrimer core. Thus, for G1-OH a total of $8 \times 3^4 = 648$ configurations can be generated. In Chart 4 we show as an example the core in "1111" arrangement and pockets in AAAA arrangement.

For G2-OH and G3-OH we can keep the assumption that the new layer of branches will adopt a configuration independent of those that the inner branches/pockets adopt. Table 6 shows

CHART 4: G1-OH Configuration Illustrating a Core "1111"−Pockets AAAA Configuration

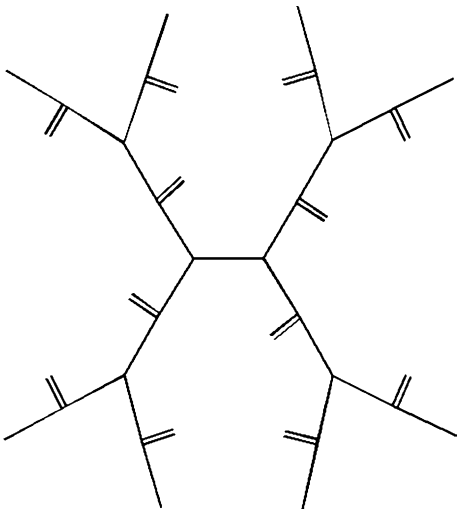

TABLE 6: Number of Distinct Configurations Expected by Considering Different Orientations of Amide O in Outer Pockets as a Function of Dendrimer Generation

generation	# configs
0	8
1	648
2	4 251 528
3	1.83×10^{14}
4	3.39×10^{29}

how many configurations will be needed given that all our assumptions hold.

These numbers might be even higher if the amide O groups are allowed to adopt a cis configuration, or lower if the configuration of a given pocket is influenced by the configuration of other pockets; however, we do not pretend to examine such cases. Even if the number of configurations calculated in Table 6 may seem overestimated, they remind us of a fact already noticed in the literature:[41] sampling in molecular dynamics or molecular mechanics becomes increasingly complex once one attempts to model accurately the multiple binding of ions/anions/water to a dendrimer. Therefore, a QM approach based on the analysis of fragments can help to narrow the configurations to a handful of feasible structures to be constructed by building QM-optimized fragments into a dendrimer. By obtaining a few geometric parameters from the QM calculations, it should be possible to characterize the pockets; this is to determine the amide O orientation that the pocket adopts when a certain molecular species is hosted.

3.3. Hydration of *Unprotonated* Outer Pocket. IR Spectral Features. As mentioned in section 2, our model of an outer pocket is made of two branches linked by a tertiary amine with a dangling methyl group instead of the branch to which it should be attached in the dendrimer. We are interested in finding the number of waters that may saturate such a pocket. Two stable configurations for the outer pocket without water were found (Figure 5). We also tried many configurations but obtained only a few local minima for a given degree of hydration, three configurations for each of the cases where one, two, three, and four water molecules are inside the pocket. All 14 configurations have been determined to be stationary points via Hessian matrix second derivative calculations.

Thermodynamic quantities for reactions 1 and 2 for $n = 0-3$ were calculated. Addition of water to an outer pocket structure is represented by

$$\mathrm{DF41}-(\mathrm{H_2O})_n + \mathrm{H_2O} \rightarrow \mathrm{DF41}-(\mathrm{H_2O})_{n+1} \qquad (1)$$

Displacement of a water molecule from a dimer (a water molecule is added to the preexistent water-in-pocket structure) is shown by

$$\mathrm{DF41}-(\mathrm{H_2O})_n + (\mathrm{H_2O})_2 \rightarrow \mathrm{DF41}-(\mathrm{H_2O})_{n+1} + \mathrm{H_2O} \qquad (2)$$

where the left-hand-side hydrated structure is chosen to be the lowest ZPE-corrected-energy configuration at a given value of n.

Selected structures included in Tables 7 and 8 were chosen on the basis of the following criteria: for $n = 0$, the three configurations yielding negative ΔG (eq 2); for $n = 1$, all four configurations found; for $n = 2$, the only one with negative ΔG (eq 2); for $n = 3$, the one with the lowest positive ΔG (eq 2). Despite the oscillations of the free energy values, there is a trend. According to eq 2 (and including data not reported), ΔG spans between −3.1 and 0.11 kcal/mol when $n = 0$, between −2.8 and 0.07 kcal/mol when $n = 1$, between −0.38 and 5.7 kcal/mol when $n = 2$, and between 2.2 and 7.5 kcal/mol when $n = 4$. Also, according to eq 2 (and considering data not reported), ΔE_0 spans between −4.9 and −1.1 kcal/mol when $n = 0$, between −5.0 and −3.0 kcal/mol when $n = 1$, between

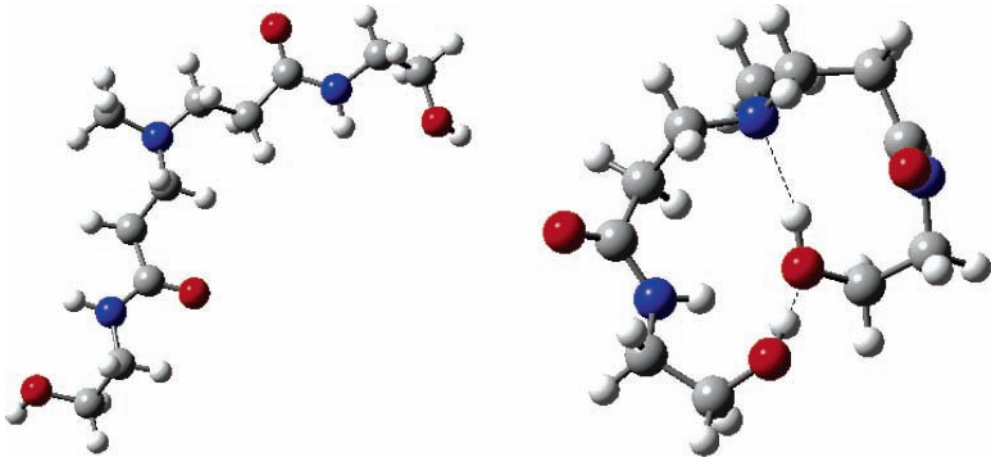

Figure 5. Reference fragments DF41. Left: RefA. Right: RefCoB with two hydrogen bonds OH···N3 (2.05 Å) and OH···OH (2.02 Å). RefCoB is chosen as the reference fragment for thermodynamic calculations because it is slightly more stable than RefA (E_0(RefCoB) − E_0(RefCoA) = −0.68 kcal/mol).

TABLE 7: Electronic Energies with ZPE Correction (ΔE_0), Enthalpies, and Free Energies of Reaction for Formation of Selected DF41−$(H_2O)_{n+1}$ Configurations According to Equation 1[a]

n	product config	ΔE_0	ΔH	ΔG
0	1C	−7.8	−8.0	−1.1
0	1D	−8.2	−9.1	1.0
0	1E	−8.9	−9.3	0.04
1	2A	−8.1	−8.9	−0.64
1	2B	−7.3	−8.2	2.1
1	2C	−9.0	−9.7	−0.82
1	2E	−6.9	−7.6	2.1
2	3A	−8.4	−9.6	1.6
3	4C	−5.3	−6.0	4.2

[a] Values are given in kcal/mol.

TABLE 8: Electronic Energies with ZPE Correction (ΔE_0), Enthalpies, and Free Energies of Reaction for Formation of Selected DF41−$(H_2O)_{n+1}$ Configurations According to Equation 2[a]

n	product config	ΔE_0	ΔH	ΔG
0	1C	−3.8	−3.4	−3.1
0	1D	−4.3	−4.5	−0.96
0	1E	−4.9	−4.7	−2.0
1	2A	−4.2	−4.4	−2.6
1	2B	−3.3	−3.6	0.14
1	2C	−5.0	−5.1	−2.8
1	2E	−3.0	−3.0	0.07
2	3A	−4.5	−5.0	−0.38
3	4C	−1.4	−1.4	2.2

[a] Values are given in kcal/mol.

−4.5 and 5.4 kcal/mol when $n = 2$, and between −1.4 and 6.1 kcal/mol when $n = 4$. Clearly the trapping of water molecules inside the pocket becomes more difficult beyond three water molecules ($n = 2$).

As discussed in section 2, the method chosen—and therefore the results—are not meant to provide exact values for the reported thermodynamic quantities which could be obtained from more intensive and expensive calculations like G2 and G3 theories.[42,43] We are rather satisfied with a qualitative description of the phenomena. Thus, configuration 2C (Table 8) is the configuration with the lowest ΔG value even though when compared to 1C and 2A the differences are small. The stability decreases when three waters are involved ($n = 2$), but even in that case the process is still favorable according to eq 2 (Table 8). However, none of the configurations is favored when four water molecules are considered ($n = 3$), not even according to eq 2. Therefore, it could be inferred from our results that *the maximum number of waters allowed by an unprotonated pocket is two*. This is in partial agreement with molecular dynamics simulation results[44] that found three as the maximum number of waters accepted per tertiary amine nitrogen (N3), however, at high pH—although we acknowledge that the comparison is not fair because the simulations were for G5-NH2 dendrimers—different from our PAMAM−OH pockets.

Optimized structures in this and the next sections suggest a classification based on three ideal configurations (outward−outward, outward−inward, and inward−inward; see Chart 3). To get insight into the configuration of the pocket upon hosting water, we gather a few relevant parameters from the optimized structure data: (1) distance between amide O atoms that provides an indication of how closed or open the pocket is; (2) distance between hydroxyl O atoms that reveals whether or not the pocket is being closed by a hydrogen bond between the −OH terminal groups; (3) the magnitude of the angle γ, which is the angle formed by the amide O1 (branch 1)−tertiary amine N3−amide O2 (branch 2); (4) angle α formed by carbonyl CO1 (branch 1)−N3−carbonyl CO2 (branch 2) to get insights into the degree of openness of the pocket. Thus, these geometric parameters, shown in Table 9, illustrate how the pocket geometric configuration accommodates to host the water molecules.

TABLE 9: Summary of Significant Bond Distances and Angles for Selected DF41−$(H_2O)_n$ Configurations

	bond distances (Å)		bond angles (deg)	
config	O−O	OT−OT	α(CO−N3−CO)	γ(O−N3−O)
RefA	7.40	12.80	120.5	120.3
RefCoB	6.80	2.98	123.2	111.3
1C	7.19	8.44	142.1	131.0
1D	5.40	4.49	122.6	95.1
1E	6.13	2.83	90.1	90.4
2A	7.16	8.45	139.8	126.7
2B	5.70	4.94	125.5	100.5
2C	7.36	8.80	144.0	133.2
2E	6.13	2.78	90.6	90.5
3A	7.12	7.27	133.3	122.0
4C	7.61	6.63	132.0	120.2

The DFT-calculated amide O−amide O (O−O) distance ranges between 5.40 and 7.61 Å, and the hydroxyl oxygen to hydroxyl oxygen distance (OT−OT) ranges from 2.98 Å (closed configurations) to 12.80 Å (open configurations). The angle α ranges between 120.5° and 144.0° and the γ angle between 90.5° and 133.2°.

The LEC (Figure 6) has both the maximum α and the maximum γ values, OT−OT distance of 8.80 Å, and O−O distance of 7.36 Å. Thus, it is mostly an outward−inward configuration. This is the trend that is observed from Table 9 for all but 1D, 2B, and 4C (configurations that are not the LECs at their corresponding degrees of hydration).

In previous work[18] we found the ratio amide I/amide II to be lower than 1.0. Such a discrepancy with the experimental trend (ratio higher than 1.0) was attributed to a lack of solvent effect in the calculated spectra. As in this work we have inserted a few explicit water molecules in dendrimer pockets, we test such an assumption by calculating the ratio amide I/amide II for the rest of the hydrated configurations (Table 10). An amide I line and an amide II line per each amide group are observed in our calculated IR spectra. However, in experiments a single band is observed. Therefore, we define a *scaled weighted average* frequency, for both amide I and amide II, resulting after a weighted average of the frequencies with the intensities used

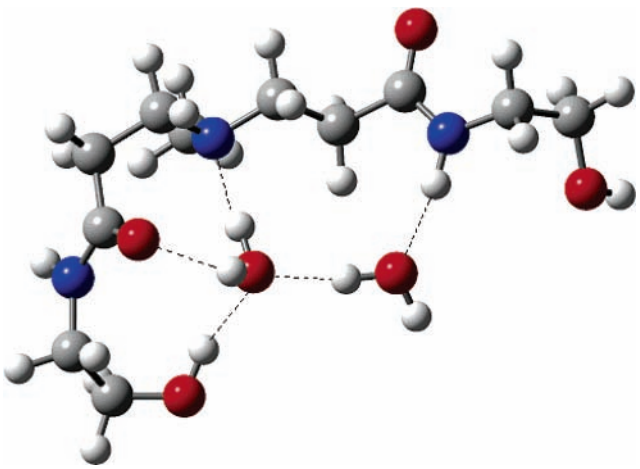

Figure 6. Lowest energy configuration (Table 8) for DF41−$(H_2O)_2$. H-bonds: $H_2O\cdots H_2O$, 1.81 Å; $OH_2\cdots N$, 1.86 Å; $OH\cdots OH_2$, 1.89 Å; $NH\cdots OH_2$, 1.93 Å; $OH_2\cdots O$, 2.06 Å.

TABLE 10: Scaled Weighted Average Amide I and Amide II Calculated Frequencies (Scale Factor 0.9614[45] for 6-31(d), Used Here for 6-31+g*), and Average Ratio of Calculated Band Intensities (Amide I/Amide II)

config	amide I	amide II	av ratio (intensities)
RefA	1672.6	1496.4	0.871
RefCoB	1689.6	1521.4	1.456
1C	1664.6	1507.6	0.859
1D	1666.7	1512.6	0.891
1E	1674.8	1546.0	1.309
2A	1665.7	1506.7	1.143
2B	1664.7	1522.9	1.135
2C	1658.7	1533.1	1.185
2E	1675.7	1530.6	1.081
3A	1665.4	1542.6	1.054
4C	1650.3	1526.9	1.360

as weighting factors. For each configuration, we calculated two ratios of intensities of amide I/amide II (one per branch) and report the average under "av ratio" in Table 10.

It is unknown to us if there is a correlation between the average ratio and the fragment configuration. For instance, RefCoB is a closed configuration with a ratio higher than 1.0, whereas RefA is an open configuration (see Figure 5) with a ratio lower than 1.0. Nonetheless, what is clear from Table 10 is that the calculated average ratio is greater than 1.0 for the RefCoB and for all selected configurations except for 1C and 1D. This suggests a low likelihood of having only one water molecule hosted in a pocket.

The frequency of the amide I is 1689.6 cm^{-1} and that of the amide II is 1521.4 cm^{-1} when the pocket hosts no water molecules. With an increase in the number of water molecules, we observe a steady shift to lower frequencies in the amide I band and to higher frequencies in amide II, a trend that is also observed experimentally.[46] These results—taken with caution because they do not represent the whole dendrimer—show that even when a complete treatment of the solvent effect is lacking, a few explicit water molecules are enough to reproduce the experimental trend found for the spectra and are more representative of the experimental spectra than the gas-phase ones previously reported.[18] Waters outside the pocket may also affect the vibrational modes of the pocket and hosted species, but we have not calculated their effect on the spectra.

3.4. Hydration of *Protonated* Outer Pocket. IR Spectral Features. Two DF41−H reference fragments were found, both binding a proton to an amide O of the adjacent branch (Figure 7). The calculated proton affinity (PA) for the most stable fragment is 244.5 kcal/mol. From the benchmark calculation done on $H\cdots N(CH_3)_3$ described in section 2, we found that the agreement with experiment is within less than 2%. Therefore, we expect a similar degree of accuracy in the reported PA values. We calculate thermodynamic quantities for reactions 4−6 for $n = 0-2$.

Addition of water to a *protonated* outer pocket structure is represented by

$$[DF41-H-(H2O)_n]^+ + H_2O \rightarrow [DF41-H-(H_2O)_{n+1}]^+ \quad (3)$$

Displacement of water from a dimer by a *protonated* outer pocket is shown by

$$[DF41-H-(H2O)_n]^+ + (H_2O)_2 \rightarrow [DF41-H-(H_2O)_{n+1}]^+ + H_2O \quad (4)$$

Equation 5 shows the addition of H_3O^+ to a *unprotonated* outer pocket structure:

$$DF41-(H2O)_n + H_3O^+ \rightarrow [DF41-((H_3O)-(H_2O)_n)]^+ \quad (5)$$

Displacement of H_3O^+ from a monohydrated hydronium by a *unprotonated* outer pocket is represented by

$$DF41-(H2O)_n + H_2O-H_3O^+ \rightarrow [DF41-((H_3O)-(H_2O)_n)]^+ + H_2O \quad (6)$$

where the left-hand-side hydrated structure is chosen to be the lowest ZPE-corrected-energy configuration at a given value of *n*.

In order to evaluate the results in Tables 12 and 13, corresponding to eq 5 and eq 6, respectively, we chose configurations of $DF41-(H_2O)_n$, for $n = 0-2$, based on their lowest energy of reaction (ΔE_0) according to eq 1. The selected configurations were 1E, 2C, and 3A along with the reference fragment DF41 (RefCoB).

Based on the magnitude of their values, reaction energies described by eqs 5 and 6 seem to describe a more likely scenario than those described by eqs 3 and 4. From Tables 12 and 13 it is evident that the most likely reactions are those where 2C* and 1B* are generated, where the proton interacts more closely with the amide oxygen, followed by 1A and 3C, where the

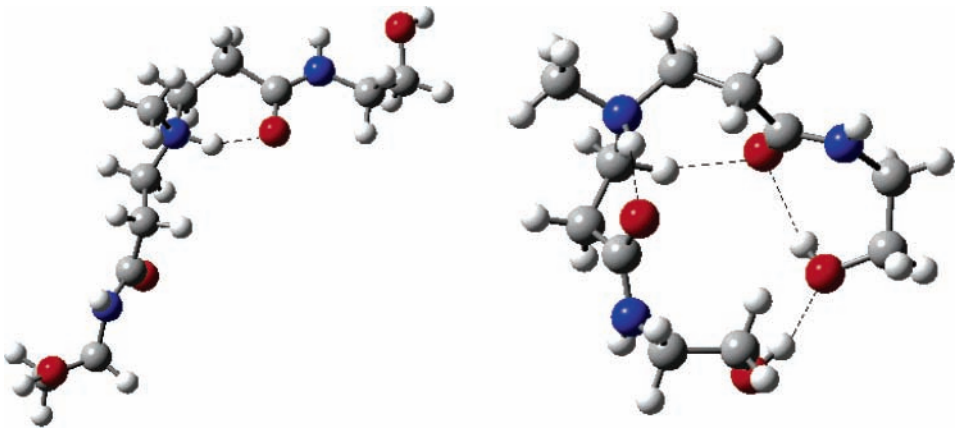

Figure 7. Protonated reference fragments DF41−H. Left: RefA. Right: RefCoB. The hydrogen bond length $NH^+\cdots O$ is 1.70 and 1.68 Å in RefA and RefCoB, respectively. For RefCoB notice that there are also three additional hydrogen bonds $OH\cdots OH$ (1.88 Å), $OH\cdots O{=}C$ (2.12 Å), and $HCH\cdots O{=}C$ (2.10 Å). RefCoB is chosen as the reference fragment because it is slightly more stable than RefA (E_0(ReCoB) − E_0(RefA) = −1.2 kcal/mol).

TABLE 11: Average Electronic Energies with ZPE Correction (ΔE_0), Enthalpies, and Free Energies of Reaction at 298.15 K for Formation of $[DF41-H-(H_2O)_{n+1}]^+$ Configurations According to Equations 3 and 4[a]

	ΔE_0		ΔH		ΔG	
n	eq 3	eq 4	eq 3	eq 4	eq 3	eq 4
1	−8.5	−4.5	−8.9	−4.3	−0.42	−2.4
2	−10.0	−6.0	−10.3	−5.8	−1.9	−3.9
3	−9.2	−5.3	−9.9	−5.3	−1.2	−3.2
av	−9.2	−5.3	−9.7	−5.1	−1.2	−3.2

[a] Values are given in kcal/mol.

TABLE 12: Electronic Energies with ZPE Correction (ΔE_0), Enthalpies, and Free Energies of Reaction for Formation of Selected $[DF41-((H_3O)-(H_2O)_n)]^+$ Configurations According to Equation 5[a]

n	product config	ΔE_0	ΔH	ΔG
0	1B*	−96.0	−96.7	−85.3
0	1D	−90.9	−91.7	−80.6
0	1A	−90.8	−90.3	−84.5
1	2C*	−99.0	−100.4	−87.5
1	2E	−91.9	−92.5	−82.2
2	3C	−93.0	−93.5	−83.9
3	4A	−91.6	−91.7	−82.5

[a] Values are given in kcal/mol.

TABLE 13: Electronic Energies with ZPE Correction (ΔE_0), Enthalpies, and Free Energies of Reaction for Formation of Selected $[DF41-((H_3O)-(H_2O)_n)]^+$ Configurations According to Equation 6[a]

n	product config	ΔE_0	ΔH	ΔG
0	1B*	−60.4	−59.9	−57.4
0	1D	−55.4	−54.8	−52.7
0	1A	−55.3	−53.4	−56.5
1	2C*	−63.4	−63.6	−59.6
1	2E	−56.4	−55.7	−54.3
2	3C	−57.4	−56.6	−56.0
3	4A	−56.0	−54.8	−54.6

[a] Values are given in kcal/mol.

pocket arms are wide open. Finally, configurations 1D and 2E are the least stable, when the pocket is closed (Figure 8).

Can higher degrees of solvation still be reached? According to Tables 12 and 13 it seems that arriving at 3C is less likely than arriving at 2C* through a pathway described by eqs 5 and 6. However, once 2C* is obtained, a pathway described by the processes in eqs 3 and 4 can follow and configuration 3C can be obtained. Thus, although the energies calculated for eqs 3 and 4 are smaller compared to those found for eqs 5 and 6, they can still make the hydration of the protonated complex possible. The effect on the geometry will be a transition from a structure (almost closed if looking at Figure 7) with an internal amide O−proton hydrogen bond (2C*) to an open structure (3C). If this is the case, then this could reflect experimental trends that have found that the dendrimer expands upon protonation.[47]

Calculated spectral features are reported in Table 14. As in the case of unprotonated pockets, the water bending modes (not shown) are also present among the amide I and amide II spectral lines. The calculated average ratio is greater than 1.0 in all configurations except 1D and 3C. Amide I ranges from 1642.6 to 1690.4 cm^{-1}, and amide II ranges from 1512.2 to 1533.0 cm^{-1}. However, no clear effect on amide I and amide II can be inferred from the results and no significant shift with respect to the unprotonated state is found.

From Table 15 it is observed that the range is 4.14−6.56 Å for the O−O distance and from 2.73 to 13.90 Å for the OT−OT distance. The magnitude of the angle α ranges from 85.7° to 139.4°, and that of the angle γ from 78.8° to 106.5°. Compared to the unprotonated pocket, the O−O distance values are shorter. The angle α ranges also around lower values although in a broader range because it covers a series of configurations: "open" with 130°−139.4°, "closed" with 85.7°−116.3°, and internal amide O−H bond with 86°−91°. The γ angle ranges around lower values, but its range of variation is similar.

At least two extreme configurations can be found: one where the amide O remains bound to the proton so that the water molecules bind outside that interaction. Configuration 2C* has the lowest OT−OT distance (they bind), its α angle is 91.0°, and γ is 101.5°, developing into a pattern that closely resembles a "outward−inward" ideal configuration. On the other hand, the wide-open configuration 3C has the maximum O−O distance, the maximum α, and the maximum γ among the configurations found, developing into a pattern that closely resembles an "inward−inward" ideal configuration (Figure 8). While the outward−inward character is the dominant pattern in unprotonated fragments, this example illustrates that there are several patterns arising when protonation occurs: inward−inward, outward−inward, and even outward−outward patterns are present.

4. Conclusions

Calculations of the most stable configurations for the tetrachloroplatinate anion and its hydrolysis products at several degrees of hydration revealed the attachment of water in equatorial positions but did not predict structures where the apical sites—above and below the Pt atom—were occupied, whereas structures with H-bond networks above the molecular plane were found as the lowest energy configurations only for the monohydrate $PtCl_3(H_2O)^-$ at the degrees of hydration tested. At low degrees of hydration, both $PtCl_3(H_2O)^-$ and *cis*-$PtCl_2(H_2O)_2$ water molecules bind more strongly in Cl−O equatorial sites whereas the weakest bound water molecules are found in Cl−Cl sites. This suggests that release of water molecules from Cl−Cl sites should occur preferentially. Obviously, no equatorial site differentiation exists for *trans*-$PtCl_2(H_2O)_2$: all four sites are Cl−O sites. Perhaps this is the reason why, at least at the degrees of hydration studied here, the trans isomer has been found more stable than the cis isomer. On the basis of this observation, we speculate that interactions between dendrimer pockets and Pt(II) complexes are more likely when the Pt(II) complex binds water in equatorial Cl−Cl sites and when the interaction is such that those water molecules are placed between the two interacting heavier molecules.

It is not possible to assert if either *cis*- or *trans*-$PtCl_2(H_2O)_2$ is more stable in aqueous solution. Our results slightly favor trans over cis, whereas a weak preference for the cis isomer should be inferred from experiments;[34] this discrepancy may arise because the number of water molecules used in our calculations is still insufficient to describe a full-solvent effect. As it is likely that both species coexist in aqueous solution, at low precursor salt concentration, both should be included in any study involving tetrachloroplatinate speciation in aqueous solution.

The second goal of this work was to determine the number of water molecules that may saturate a pocket. Given our definition of outer pocket and its molecular modeling, we notice that no more than two—perhaps three—water molecules are needed to saturate an outer pocket when such pocket is unprotonated, which is inferred from calculated thermodynamic

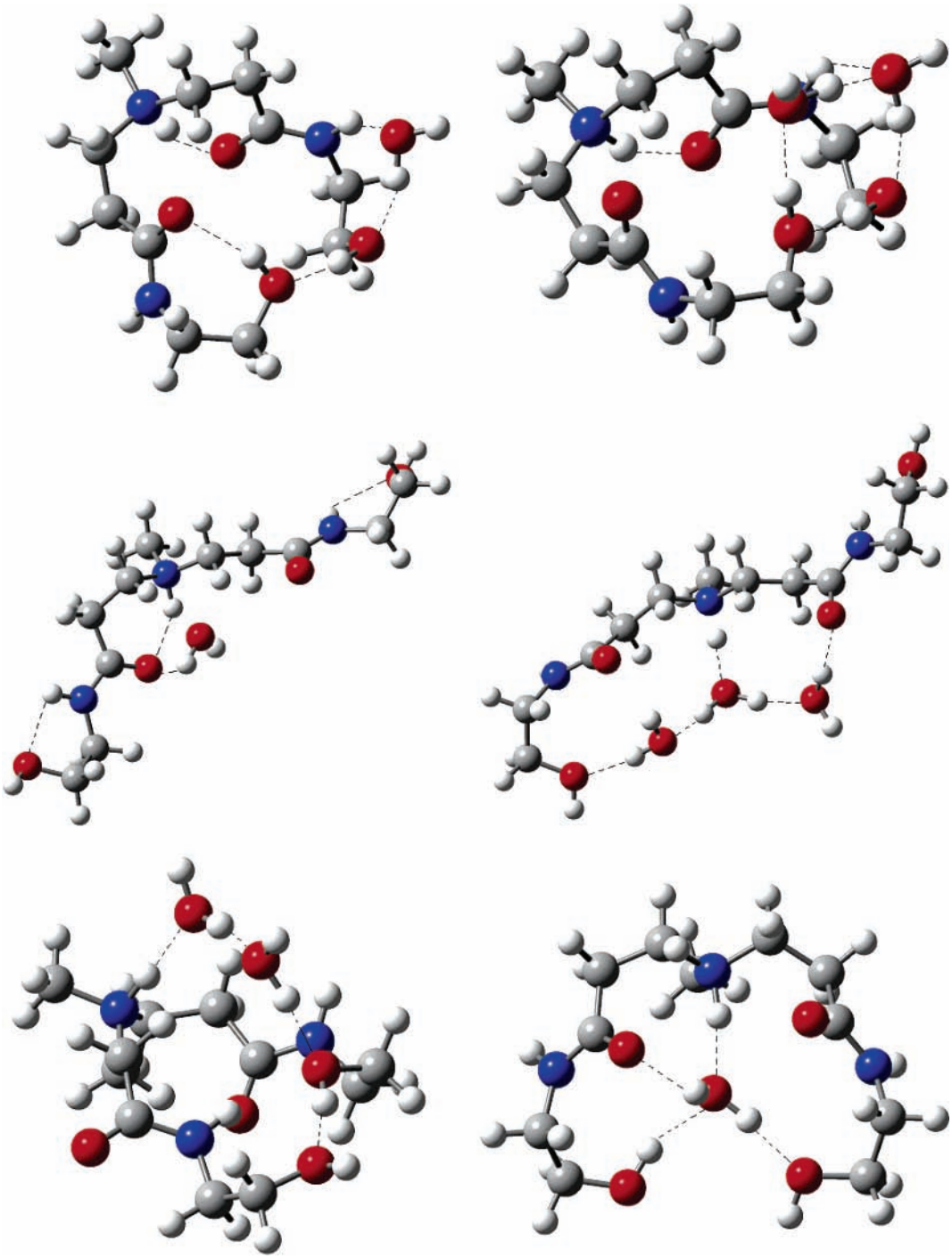

Figure 8. Upper left: configuration 1B*. Upper right: configuration 2C*. Notice clearly the H-bond between the proton located at the tertiary amine N site and the amide O atom, configurations where the pocket arms are wide open. Middle left: configuration 1A. Middle right: configuration 3C. Configurations where the pocket appears closed and the amide O−proton H-bond is absent. Lower left: configuration 2E. Lower right: configuration 1D.

and IR data. Such a number could not be accurately determined for a protonated pocket, because under these conditions the dendrimer can adopt a more open configuration. These calculations also provide the reference structure, namely DF41−$(H_2O)_2$ (configuration 2C) for thermodynamic calculations of noncovalent binding reactions with Pt(II) complexes to be reported elsewhere.

An analysis of possible pocket configurations done on the basis of the orientations of the amide O atoms in outer pockets provides an estimate of the number of total configurations that may be expected for low generation dendrimers, thus highlighting the impracticality of simulations with larger dendrimers. Besides, a geometric analysis of the structure of an outer pocket is proposed to establish the possible conformations of a water-containing outer pocket. Configurations having combinations of amide O atoms pointing outward or inward with respect to the pocket are identified. While the outward−inward character is the dominant pattern in unprotonated fragments, several patterns arise when protonation occurs: inward−inward, outward−inward, and even outward−outward patterns are present. However, a transition from a configuration that closely resembles an ideal "outward−inward" to another that is more of an "inward−inward", yet open to accept more water inside the pocket, is expected to take place in protonated pockets. As

TABLE 14: Scaled Weighted Average Amide I and Amide II Calculated Frequencies (Factor 0.9614[45] for 6-31(d), Used Here for 6-31+g*), Average Ratio of Calculated Band Intensities (Amide I/Amide II)

config	amide I	amide II	av ratio (intensities)
RefA	1659.4	1512.2	1.572
RefCoB	1642.6	1520.4	1.838
1B*	1643.1	1533.0	1.344
1D	1688.2	1518.1	0.943
1A	1660.9	1513.4	1.171
2C*	1654.0	1531.2	1.255
2E	1690.4	1522.5	1.549
3C	1664.1	1514.3	0.734

TABLE 15: Summary of Significant Bond Distances and Angles for $[DF41-H-(H_2O)_n]^+$ Configurations

		bond distances (Å)		bond angles (deg)	
n	config	O−O	OT−OT	α(CO−N3−CO)	γ(O−N3−O)
0	RefA	5.38	13.70	128.2	102.8
0	RefCoB	4.23	2.83	85.8	87.3
1	1B*	4.14	2.78	86.0	85.5
1	1D	4.18	4.04	116.3	78.8
1	1A	5.45	13.90	130.0	102.7
2	2C*	4.77	2.73	91.0	101.5
2	2A	5.73	10.10	121.2	102.8
2	2E	5.41	2.76	85.7	81.8
3	3C	6.56	13.20	139.4	106.5
3	3A	5.63	7.98	113.5	96.1
4	4A	6.42	11.72	139.3	104.7

pockets are part of dendrimers, this shift in conformation upon protonation of tertiary amine should impact the configuration of larger dendrimers to the extent that such protonation occurs in those systems. Therefore, these results suggest a swelling upon protonation as observed experimentally.[47]

The effect of explicit solvent molecules on the infrared spectra of the outer dendrimer pockets shows a change in the intensity ratio amide I/amide II with respect to gas-phase results, resulting in better agreement with reported experimental data, particularly for unprotonated pockets.

Acknowledgment. This work was partially supported by the National Science Foundation Grant CTS-0103135 and by the Department of Energy Grant DE-FG02-05ER15729. Supercomputer time granted by the National Energy Research Scientific Computing Center (NERSC), and by the DoD Major Shared Resource Centers (ARL MSRC and ASC MSRC), is gratefully acknowledged.

Supporting Information Available: Tables of hydration data and calculated structures. This material is available free of charge via the Internet at http://pubs.acs.org.

References and Notes

(1) Cahen, D.; Hodes, G. Molecules and Electronic Materials. *Adv. Mater.* **2002**, *14*, 789−798.

(2) Narayanan, R.; El-Sayed, M. A. Catalysis with Transition Metal Nanoparticles in Colloidal Solution: Nanoparticle Shape Dependence and Stability. *J. Phys. Chem. B* **2005**, *109*, 12663−12676.

(3) Cushing, B. L.; Kolesnichenko, V. L.; O'Connor, C. J. Recent Advances in the Liquid-Phase Synthesis of Inorganic Nanoparticles. *Chem. Rev.* **2004**, *104*, 3893−3946.

(4) Crooks, R. M.; Zhao, M.; Sun, L.; Chechik, V.; Yeung, L. K. Dendrimer-encapsulated Metal Nanoparticles: Synthesis, Characterization, and Applications to Catalysis. *Acc. Chem. Res.* **2001**, *34*, 181−190.

(5) Scott, R. W. J.; Datye, A. K.; Crooks, R. M. Bimetallic Palladium-Platinum Dendrimer-Encapsulated Catalysts. *J. Am. Chem. Soc.* **2003**, *125*, 3708−3709.

(6) Xie, H.; Gu, Y. L.; Ploehn, H. J. Dendrimer-mediated synthesis of platinum nanoparticles: new insights from dyalisis and atomic force microscopy measurements. *Nanotechnology* **2005**, *16*, S492−S501.

(7) Esumi, K.; Isono, R.; Yoshimura, T. Preparation of PAMAM- and PPI- Metal (Silver, Platinum, and Palladium) Nanocomposites and Their Catalytic Activities for Reduction of 4-Nitrophenol. *Langmuir* **2004**, *20*, 237−243.

(8) Yang, L.; Luo, Y.; Jia, X.; Ji, Y.; You, L.; Zhou, Q. Preparation of Monodisperse Platinum Nanocrystal Core-Poly(amidoamine) (PAMAM) Dendrimer Shell Structures as Monolayer Films. *J. Phys. Chem. B* **2004**, *2004*, 1176−1178.

(9) Chung, Y.-M.; Rhee, H.-K. Pt-Pd bimetallic nanoparticles encapsulated in dendrimer nanoreactor. *Catal. Lett.* **2003**, *85*, 159−164.

(10) Fu-Ren, F. F.; Mazzitelli, C. L.; Brodbelt, J. S.; Bard, A. J. Electrochemical, Spectroscopic, and Mass Spectrometric Studies of the Interaction of Silver Species with Polyamidoamine Dendrimers. *Anal. Chem.* **2005**, *77*, 4413−4422.

(11) Zheng, J.; Dickson, R. M. Individual Water-Soluble Dendrimer-Encapsulated Silver Nanodot Fluorescence. *J. Am. Chem. Soc.* **2002**, *124*, 13982−13983.

(12) Zheng, J.; Petty, J. T.; Dickson, R. M. High Quantum Yield Blue Emission from Water-Soluble Au_8 Nanodots. *J. Am. Chem. Soc.* **2003**, *125*, 7780−7781.

(13) Campbell, C. T.; Parker, S. C.; Starr, D. E. The Effect of Size-Dependent Nanoparticle Energetics on Catalyst Sintering. *Science* **2002**, *298*, 811−814.

(14) Schalow, T.; Brandt, B.; Starr, D. E.; Laurin, M.; Schauermann, S.; Shaikhutdinov, S. K.; Libuda, J.; Freund, H.-J. Oxygen-induced restructuring of a Pd/Fe_3O_4 model catalyst. *Catal. Lett.* **2006**, *107*, 189−196.

(15) Cakara, D.; Kleimann, J.; Borkovec, M. Microscopic protonation equilibria of poly(amidoamine) dendrimers from macroscopic titrations. *Macromolecules* **2003**, *36*, 4201−4207.

(16) Lang, H.; May, R. A.; Iversen, B. L.; Chandler, B. D. Dendrimer-Encapsulated Nanoparticle Precursors to Supported Platinum Catalysts. *J. Am. Chem. Soc.* **2003**, *125*, 14832−14836.

(17) Niu, Y.; Sun, L.; Crooks, R. M. Determination of the Intrinsic Proton Binding Constants for Poly(amidoamine) Dendrimers via potentiometric pH Titration. *Macromolecules* **2003**, *36*, 5725−5731.

(18) Tarazona-Vasquez, F.; Balbuena, P. B. Ab initio study of the lowest energy conformers and IR spectra of poly(amidoamine)-G0 dendrimers. *J. Phys. Chem. B* **2004**, *108*, 15982−15991.

(19) Tarazona-Vasquez, F.; Balbuena, P. Dendrimer-Tetrachloroplatinate Precursor Interactions 2. Noncovalent Binding in PAMAM Outer Pockets. *J. Phys. Chem. B* **2007**, *111*, 945−953.

(20) Hay, P. J.; Wadt, W. R. Ab initio effective core potentials for molecular calculations. Potentials for the transition metal atoms Sc to Hg. *J. Chem. Phys.* **1985**, *82*, 270−283.

(21) Hunter, E. P.; Lias, S. G. Evaluated Gas Phase Basicities and Proton Affinities of Molecules: An Update. *J. Phys. Chem. Ref. Data* **1998**, *27*, 413−656.

(22) Blades, A. T.; Jayaweera, P.; Ikonomou, H. G.; Kebarle, P. Ion-Molecule Clusters involving doubly charged metal ions (M2+). *Int. J. Mass. Spectrom. Ion Processes* **1990**, *102*, 251−267.

(23) Raber, J.; Zhu, C.; Eriksson, L. A. Theoretical Study of Cisplatin Binding to DNA: The Importance of Initial Complex Stabilization. *J. Phys. Chem. B* **2005**, *109*, 11006−11015.

(24) Gitsov, I.; Frechet, J. M. J. Stimuli-Responsive Hybrid Macromolecules: Novel Amphiphilic Star Copolymers With Dendritic Groups at the Periphery. *J. Am. Chem. Soc.* **1996**, *118*, 3785−3786.

(25) Tarazona-Vasquez, F.; Balbuena, P. Complexation of Cu(II) Ions with the Lowest Generation Poly(amido-amine)-OH Dendrimers: A Molecular Simulation Study. *J. Phys. Chem. B* **2005**, *109*, 12480−12490.

(26) Frisch, M. J.; Trucks, G. W.; Schlegel, H. B.; Scuseria, G. E.; Robb, M. A.; Cheeseman, J. R.; Montgomery, J. A., Jr.; Vreven, T.; Kudin, K. N.; Burant, J. C.; Millam, J. M.; Iyengar, S. S.; Tomasi, J.; Barone, V.; Mennucci, B.; Cossi, M.; Scalmani, G.; Rega, N.; Petersson, G. A.; Nakatsuji, H.; Hada, M.; Ehara, M.; Toyota, K.; Fukuda, R.; Hasegawa, J.; Ishida, M.; Nakajima, T.; Honda, Y.; Kitao, O.; Nakai, H.; Klene, M.; Li, X.; Knox, J. E.; Hratchian, H. P.; Cross, J. B.; Bakken, V.; Adamo, C.; Jaramillo, J.; Gomperts, R.; Stratmann, R. E.; Yazyev, O.; Austin, A. J.; Cammi, R.; Pomelli, C.; Ochterski, J. W.; Ayala, P. Y.; Morokuma, K.; Voth, G. A.; Salvador, P.; Dannenberg, J. J.; Zakrzewski, V. G.; Dapprich, S.; Daniels, A. D.; Strain, M. C.; Farkas, O.; Malick, D. K.; Rabuck, A. D.; Raghavachari, K.; Foresman, J. B.; Ortiz, J. V.; Cui, Q.; Baboul, A. G.; Clifford, S.; Cioslowski, J.; Stefanov, B. B.; Liu, G.; Liashenko, A.; Piskorz, P.; Komaromi, I.; Martin, R. L.; Fox, D. J.; Keith, T.; Al-Laham, M. A.; Peng, C. Y.; Nanayakkara, A.; Challacombe, M.; Gill, P. M. W.; Johnson, B.; Chen, W.; Wong, M. W.; Gonzalez, C.; Pople, J. A. *Gaussian03*, revision C.02; Gaussian, Inc.: Wallingford, CT, 2004.

(27) Ohba, S.; Sato, S.; Saito, Y.; Ohshima, K.; Harada, J. Electron-Density Distribution in Crystals of Potassium Tetrachloroplatinate(II) and Influence of X-Ray Diffuse-Scattering. *Acta Crystallogr.* **1983**, 49−53.

(28) Ayala, R.; Sanchez, Marcos, E.; Diaz-Moreno, S.; A., S. V.; Munoz-Paex, A. Geometry and Hydration Structure of Pt(II) Square Planar Complexes [Pt(H2O)4]2+ and [PtCl4]2- as Studied by X-ray Absorption

Spectroscopies and Quantum-Mechanical Computations. *J. Phys. Chem. B* **2001**, *105*, 7588−7593.

(29) Torrico, F.; Pappalardo, R. R.; Sanchez, Marcos, E.; Martinez, J. M. Hydration structure and dynamic properties of the square planar Pt(II) aquaion compared to the Pd(II) case. *Theor. Chem. Acc.* **2006**, *115*, 196−203.

(30) Purans, J.; Fourest, B.; Cannes, C.; Shadkov, V.; Venault, D. L.; Lecomte, M. Structural Investigation of Pd(II) in Concentrated Nitric and Perchloric Acid Solutions by XAFS. *J. Phys. Chem. B* **2005**, *109*, 11074−11082.

(31) Caminiti, R.; Carbone, M.; Sadun, C. Palladium (II) and platinum (II) aqueous solutions. Evidence for the solvation of the $[PdCl4]^{2-}$ and $[PtCl4]^{2-}$ ions. *J. Mol. Liq.* **1998**, *75*, 149−158.

(32) Deeth, R. J.; Elding, L. I. Theoretical Modeling of Water Exchange on $[Pd(H_2O)_4]^{2+}$, $[Pt(H_2O)_4]^{2+}$, and trans-$[PtCl_2(H_2O)_2]$. *Inorg. Chem.* **1996**, *35*, 5019−5026.

(33) Bengtsson, L. A.; A., O. Intermolecular Effects On The Geometry Of $[PtCl4]^{2-}$—X-Ray-Diffraction Studies Of Aqueous H_2PtCl_4 And Crystalline $(NH_4)_2PtCl_4$. *Acta Chem. Scand.* **1992**, *46*, 707−711.

(34) Elding, L. I. Stepwise Dissociation Of Tetrachloroplatinate(II) Ion In Aqueous Solution 6. Rates Of Formation And Equilibria Of Chloro Aqua Complexes Of Platinum(II). *Acta Chem. Scand.* **1970**, *24*, 1527.

(35) Hush, N. S.; Schamberger, J.; Backsay, G. B. A quantum chemical computational study of the relative stabilities of cis- and trans-platinum dichloride in aqueous solution. *Coord. Chem. Rev.* **2005**, 249.

(36) Bitetti-Putzer, R.; Dinner, A. R.; Yang, W.; Karplus, M. Conformational sampling via a self-regulating effective energy surface. *J. Chem. Phys.* **2006**, *124*, 174901.

(37) Carloni, P.; Rothlisberger, U.; Parrinello, M. The Role and Perspective of Ab Initio Molecular Dynamics in the Study of Biological Systems. *Acc. Chem. Res.* **2002**, *35*, 455−464.

(38) Simonson, T.; Archontis, G.; Karplus, M. Free Energy Simulations Come of Age: Protein-Ligand Recognition. *Acc. Chem. Res.* **2002**, *35*, 430−437.

(39) Bartels, C.; Schaefer, M.; Karplus, M. Determination of equilibrium properties of biomolecular systems using multidimensional adaptive umbrella sampling. *J. Chem. Phys.* **1999**, *111*, 8048−8067.

(40) VandeVondele, J.; Rothlisberger, U. Efficient multidimensional free energy calculations for ab initio molecular dynamics using classical bias potentials. *J. Chem. Phys.* **2000**, *113*, 4863−4868.

(41) Maiti, P. K.; Cagin, T.; Wang, G.; Goddard, W. A. Structure of PAMAM Dendrimers: Generations 1 through 11. *Macromolecules* **2004**, *37*, 6236−6254.

(42) Curtiss, L. A.; Raghavachari, K.; Trucks, G. W.; Pople, J. A. Gaussian-2 theory for molecular energies of first- and second- row compounds. *J. Chem. Phys.* **1991**, *94*, 7221−7230.

(43) Curtiss, L. A.; Raghavachari, K.; Redfern, P. C.; Rassolov, V.; Pople, J. A. Gaussian-3 (G3) Theory for Molecules Containing First and Second-Row Atoms. *J. Chem. Phys.* **1998**, *109*, 7764−7776.

(44) Maiti, P. K.; Cagin, T.; Lin, S.-T.; Goddard, W. A. Effect of Solvent and pH on the Structure of PAMAM Dendrimers. *Macromolecules* **2005**, *38*, 979−991.

(45) Scott, A. P.; Radom, L. Harmonic vibrational frequencies: An evaluation of Hartree-Fock, Moller-Plesset, quadratic configuration interaction, density functional theory, and semiempirical scale factors. *J. Phys. Chem.* **1996**, *100*, 16502−16513.

(46) Kubelka, J.; Huang, R.; Keiderling, T. A. Solvent Effects on IR and VCD Spectra of Helical Peptides: DFT-Based Static Spectral Simulations with Explicit Water. *J. Phys. Chem. B* **2005**, *109*, 8231−8243.

(47) Betley, T. A.; Banaszak Holl, M. M.; Orr, B. G.; Swanson, D. R.; Tomalia, D. A.; Baker, J. R., Jr. Tapping Mode Atomic Force Microscopy Investigation of Poly(amidoamine) Dendrimers: Effects of Substrate and pH on Dendrimer Deformation. *Langmuir* **2001**, *17*, 2768−2773.